

2003-2018 Monitoring of the Crab Nebula Polarization in hard X-rays with *INTEGRAL* SPI.

E. JOURDAIN¹ AND J.-P. ROQUES¹

¹ *CNRS; IRAP; 9 Av. colonel Roche, BP 44346, F-31028 Toulouse cedex 4, France*
Université de Toulouse; UPS-OMP; IRAP; Toulouse, France

ABSTRACT

We have analyzed 16 years of observations dedicated to the Crab(pulsar + nebula) with the *INTEGRAL* SPI instrument to investigate its polarization properties. We find that the source presents a substantially polarized emission (PF = 24%) in the hard X-ray domain, with the electric vector aligned with the pulsar spin axis, in agreement with other results at various wavelengths. The stability of the polarization characteristics with energy and over the 16 years covered by the data is remarkable, completing the standard candle status of the source in the spectral domain. The polarization measurements imply that the synchrotron emission is the dominant mechanism of photon production from radio to hard X-rays. The high level of polarized emission points out the steadiness of the source, in particular of the magnetic field configuration and geometry.

Keywords: polarization; X-rays: individual (Crab); gamma-rays: individual (Crab); radiation mechanisms: non-thermal

1. INTRODUCTION

SPI is a hard X-ray/soft γ -ray spectrometer providing an excellent energy resolution in the 20 keV-8 MeV energy range with some imaging capabilities. In addition, the design of the detector plane, with 19 independent crystals, makes possible the measurement of the polarization parameters of the incident radiation, for energies above ~ 100 keV. Indeed, [Dean et al. \(2008\)](#) have analyzed the SPI data of the Crab pulsar (off-pulse emission) and reported the first detection of a polarized emission in the hard X-ray domain. Then, [Forot et al. \(2008\)](#) confirm the polarization of the Crab emission with the imager IBIS, also aboard the *INTEGRAL* mission. Since, several instruments followed the way, enlarging the investigated energy domain. In this paper, we analyzed the SPI data accumulated on the Crab nebula since the launch of the *INTEGRAL* mission. The large amount of data allows us to study the polarization characteristics of the source emission both over the time and as a function of the energy.

2. OBSERVATIONS AND DATA ANALYSIS

In this section, we will focus on the information specifically relevant to the polarimetry study. The reader can refer to [Vedrenne et al. \(2003\)](#) for an overview of the SPI instrument and to [Roques et al. \(2003\)](#) for the in flight performance, while a description of the standard data analysis can be found in [Jourdain & Roques \(2009\)](#) and [Roques & Jourdain \(2019\)](#).

2.1. *The Data set*

Since its launch, the *INTEGRAL* observatory performs regular observations of the Crab nebula, to allow calibration monitoring/updates of the onboard instruments. These observations are performed twice a year, in February-March, then in September. The first campaign in March 2003, just after the end of the mission performance validation phase, gathered 446 ks of data (useful duration; Revolutions 43-44-45). After that, the bi-annual campaigns consisted of relatively short exposures (~ 50 ks), often dedicated to peculiar configuration tests (off-axis pointings, mask corner study...). Since 2008, each calibration campaign lasts 2 revolutions, i.e. ~ 400 ks, twice a year, with, in general, a standard 5X5 pattern pointing strategy. In addition, shorter observations (45 ks) are planned every 4 revolutions all along the Crab visibility periods, but these will not be considered in the following. Before starting our analyses, the exposures which present unstable background or other issues (pointing anomaly, outburst of the neighboring source A0535+262, etc.) have been removed. The final data set encompasses ~ 6.4 Ms, from March 2003 to September 2018. Further, to seek for any source evolution, the data set has been split into four periods, as a compromise between a timescale as short as possible, and an adequate signal to noise ratio. Due to the lack of suitable observations between March 2003 and October 2005, we consider separately the March 2003 revolutions. The remaining dataset has been broken up into three parts of similar useful durations (see Table 1). These four sub-data sets will be referred to with their respective labels, P1 to P4, in the subsequent analyses.

2.2. *SPI as a Polarimeter*

The SPI polarimetric capacities rely on the Compton interactions of high energy photons in the detection plane. This latter consists of 19 Germanium crystals, and photons above ~ 100 keV may diffuse in a first crystal and escape toward another one, where a second interaction occurs and so on, until a photo-electric absorption or final escaping. These events are called 'multiple event' (hereafter ME). The characteristics of the energy deposits and detectors involved contain crucial information on the polarization properties of the incident photons. In Germanium detectors, the fraction of ME (i.e. Compton interactions with the diffused photon escaping toward the next detector) becomes non negligible above ~ 90 keV. However, ME remain minoritarian and represent only $\sim 20\%$ of the total incident flux integrated above 100 keV. In fact, most of the Compton diffused photons are photo-absorbed in the same detector. This low efficiency implies long integration durations to obtain a good signal-to-noise ratio.

In practice, we consider only photons which hit two adjacent detectors (double events or ME2). This turns out to handle 42 pseudo-detectors (42 possible pairs of adjacent detectors), instead of 19 detectors as done in the standard analysis. Concerning the spectra and light curve production, the standard analysis tools, used routinely for reconstructing the incident flux from 'single detector' events (SE and PE¹.) can be applied to ME2 events. The appropriate response matrices have been produced, together with the standard matrices (Sturmer et al. 2003), and the flux extraction procedure is the same. To validate the ME2 fluxes which are considered in the polarimetry study described below, we build the corresponding spectra by deconvolving the ME2 counts with relevant matrices and compare them to the single detector event spectra.

¹ SE and PE flags correspond to events which loss energy in only one detector (Single detector Events). If such an event triggers a second specific electronic chain (PSD module, dedicated to a pulse shape analysis), it is flagged PE, if not, it is flagged SE. See Roques & Jourdain (2019) for details

The procedure specifically developed for the polarization studies has been detailed in [Chauvin et al. \(2013\)](#). The main features are:

- Selection of ME2 events in the 42 pseudo-detectors: Each pseudo-detector is associated with the total energy deposit (sum of the two measured energies).
- Simulations of the instrument responses to a polarized emission, for 17 polarization angles (PA, from 0° to 170° by step of 10°), and 100 polarization fractions (PF, 0% to 100% by step of 1%), considering the Crab localization in the FoV, for each pointing.
- Comparison of simulations and observational data, for a given set of pointings: Source and background normalizations are estimated by the resolution of an equation system for each (PA, PF) pair.

$$D_{sd} = x \times G_{sd}(PF, PA) + y \times B_{sd} \quad (1)$$

where D_{sd} is the observed count distribution for a science window (or exposure) s , in the pseudo-detector d ; x is the source normalisation; G_{sd} , the simulated count distribution, for the same s and d , as a function of the source polarization fraction, PF, and angle, PA; y is the background normalization and B_{sd} , the background spatial distribution, taken from an empty field observation. The simulated counts are renormalized to the corresponding detector livetimes. The x and y values are determined through a linear least-squares resolution and the resulting χ^2 value is stored. At the end of the PA and PF loops, the lower χ^2 between model and data identifies the best parameters.

3. RESULTS

3.1. *spectral analysis*

A spectral analysis from both single and multiple events has been performed, in order to compare the respective averaged spectra. For each of the four periods mentioned above, both spectra have been fit simultaneously. The Crab nebula emission has been described by the Band model (GRBM in Xspec language), proposed by [Band et al. \(1993\)](#) to model the GRB spectra. This analytical model reproduces the smooth curvature observed between 20 and ~ 1 MeV better than a broken power law ([Roques & Jourdain 2019](#)). The same synchrotron origin of both GRB and pulsar emissions further supports this choice. For each period, the shape parameters have been coupled between both spectra, while the individual normalizations are kept free. The results of the spectral analyses are presented in [Table 2](#) and [Figure 1](#). Furthermore, the normalization factors (for $E \simeq 170$ keV) agree within 5% in any period. The data below $\simeq 170$ keV suffer from the uncertainties in the ME2 efficiency embedded in the response matrices. These inaccuracies do not affect the polarization results since they have no specific anisotropy on the detector plane. Finally, the perfect agreement between both spectra for each period demonstrates the reliability of the ME2 flux extraction.

3.2. *Polarization study*

Once the ME2 events were validated, the procedure described in the previous section has been applied to the total data set. We have selected photons with energies between 130 and 436 keV, in order to optimize the signal-to-noise ratio. Note that the events between 196 and 201 keV have been removed, due to the strong background line present at 198 keV. Assuming constant values all along the 16 years, we obtain a Polarization Angle (PA) of $120^\circ \pm 6^\circ$ with a Polarization Fraction (PF) of

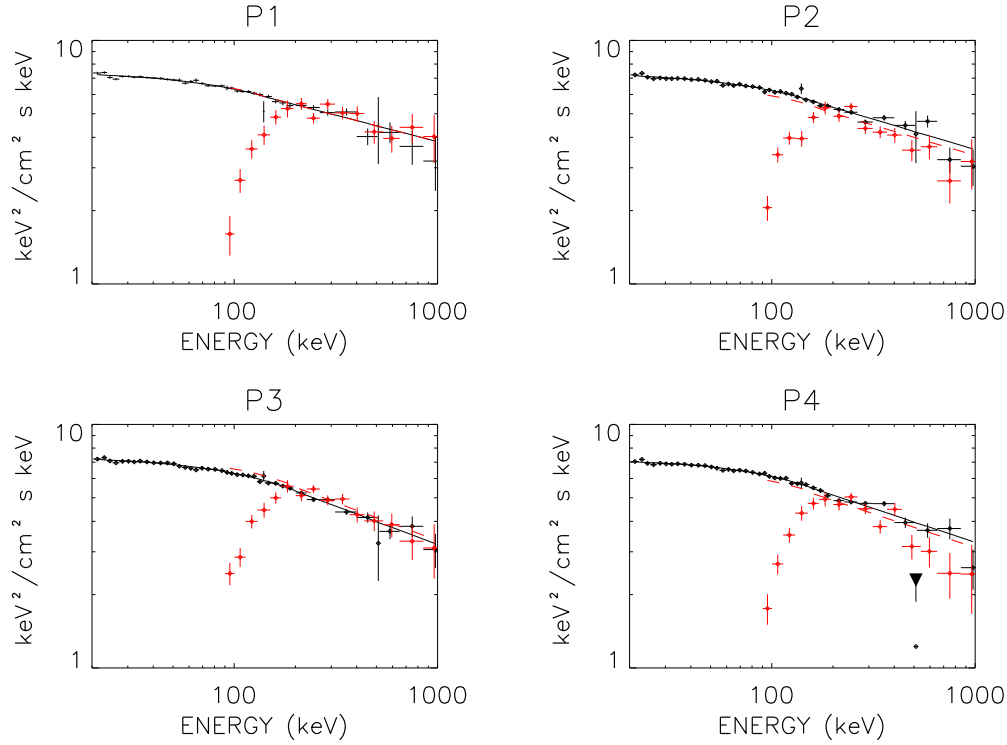


Figure 1. Spectra extracted from SE+PE (black points) and ME2 (red points) for the four periods described in Table 1.

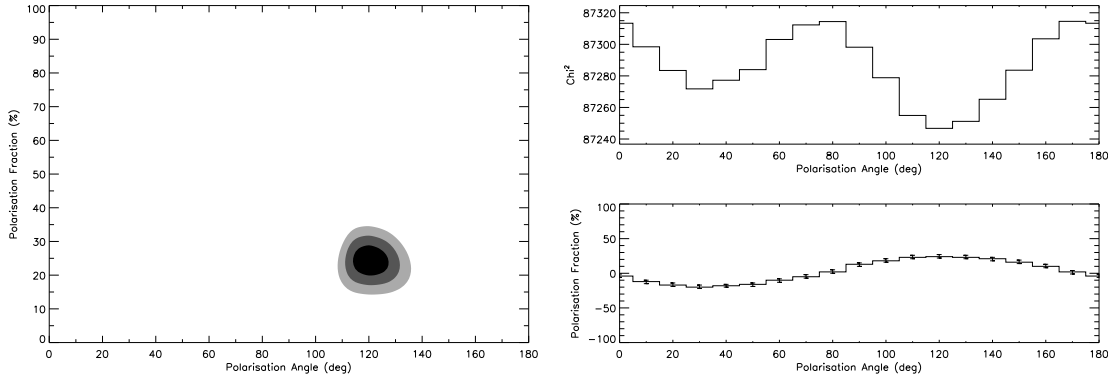


Figure 2. Best-fit polarization parameters of the Crab nebula, between 130 and 436 keV, for the 6.4 Ms data set, from 2003 to 2018. Left: significance contours in the PA-PF plane, for $\chi^2_{min} + 2.7$, 6.18 and 11.8, i.e. 1, 2 and 3 σ confidence levels. Right: Minimum χ^2 (top) and associated FP (bottom) in function of PA

$24 \pm 4\%$. This result is visualized in Figure 2, in the PA-PF plane, with the 2-D surface contours calculated from the χ^2 map, at $\chi^2_{min} + 2.7$, 6.18 and 11.8, corresponding to 1, 2 and 3 σ confidence levels for two free parameters.

To verify the stability of the source over time, the same analysis has been performed separately for periods P1 to P4. The individual results are displayed in Figure 3. In Figure 4, the evolution of the best fit polarization parameters are plotted, and compared to the mean values, obtained from the

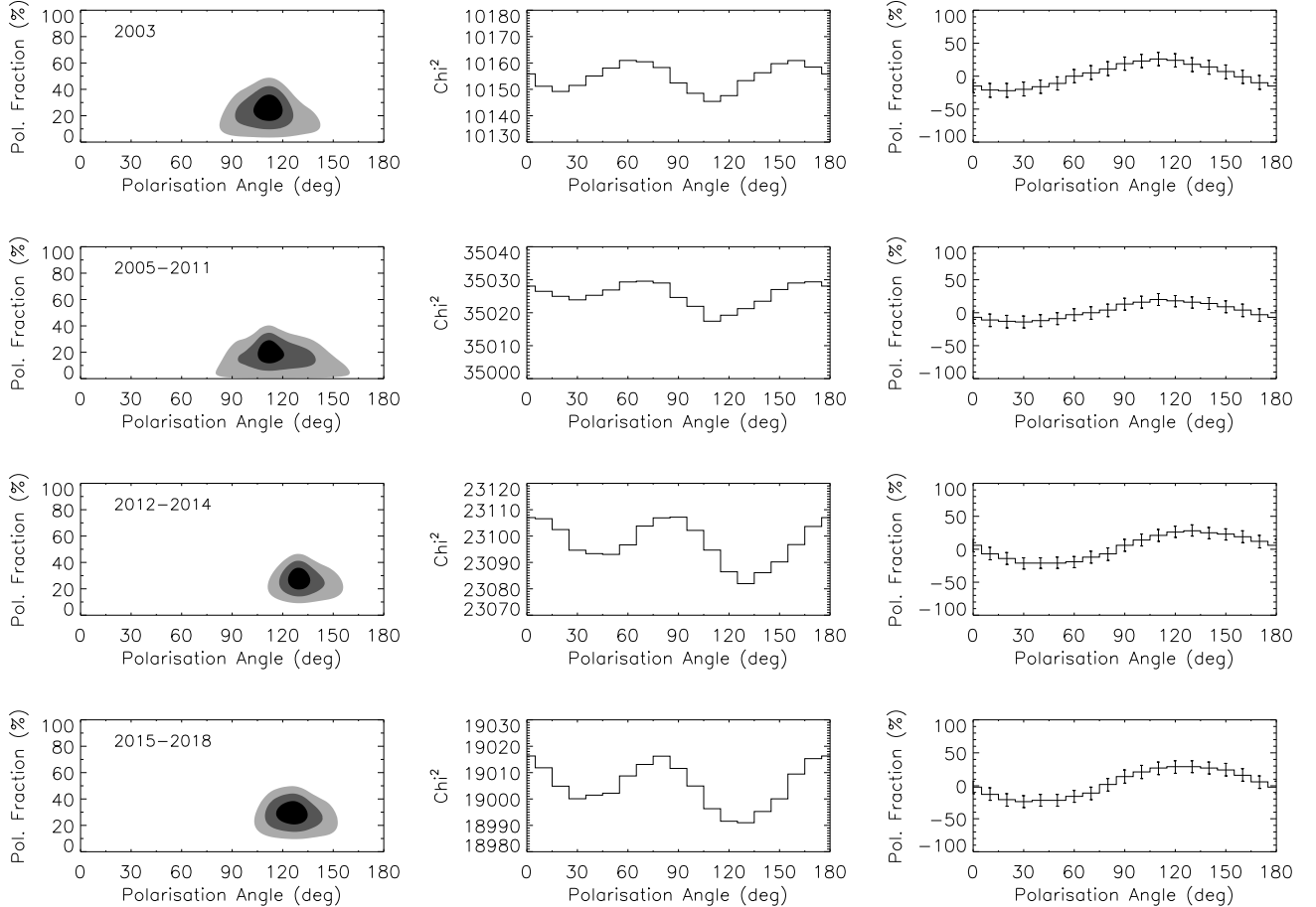


Figure 3. The same as Figure 2, for the four periods defined in Table 1.

total data set (dashed lines = 1σ uncertainty interval). No significant evolution is visible, all values being compatible with the respective mean values.

To complete our study, we have investigated the polarization characteristics of the source over energy. The global energy band (130-436 keV) has been split into 3 energy bins : 130-196 keV, 201-313 keV and 313-436 keV. The polarization parameters have been determined for each bin, for the total data set. The individual results are displayed in Figure 5, while the evolution of the parameters with energy is shown in Figure 6, together with the result from the total energy range as reference (dashed lines = 1σ uncertainty interval). The Polarization Angle as well as the Polarization Fraction appear, once again, very stable.

4. DISCUSSION AND CONCLUSION

With the SPI spectrometer aboard *INTEGRAL*, we benefit from a large amount of observations in the hard X-ray domain, dedicated to an emblematic source, the Crab nebula. Particularly interesting is the possibility to investigate the polarization properties of this source, for the last 16 years. In the considered energy range (above 100 keV), the polarimetry studies are less straightforward than in optic or radio. Concerning SPI, these measurements are based on the Compton interactions of the high energy photons in the detector plane. During a Compton interaction, the polarization of

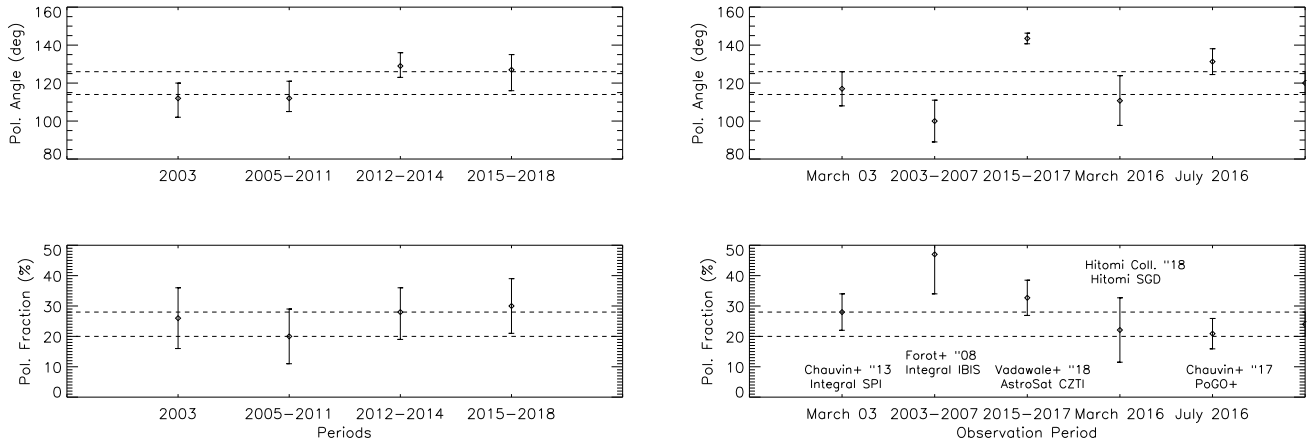


Figure 4. Left: Evolution of the SPI polarization parameters with time, in the 130-436 keV energy range. The errors quoted are 1σ for 2 parameters of interest. Right: Results from various instruments (references in the text). In both panels, dashed lines represent the 1σ uncertainty interval for our SPI total data set best-fit values.

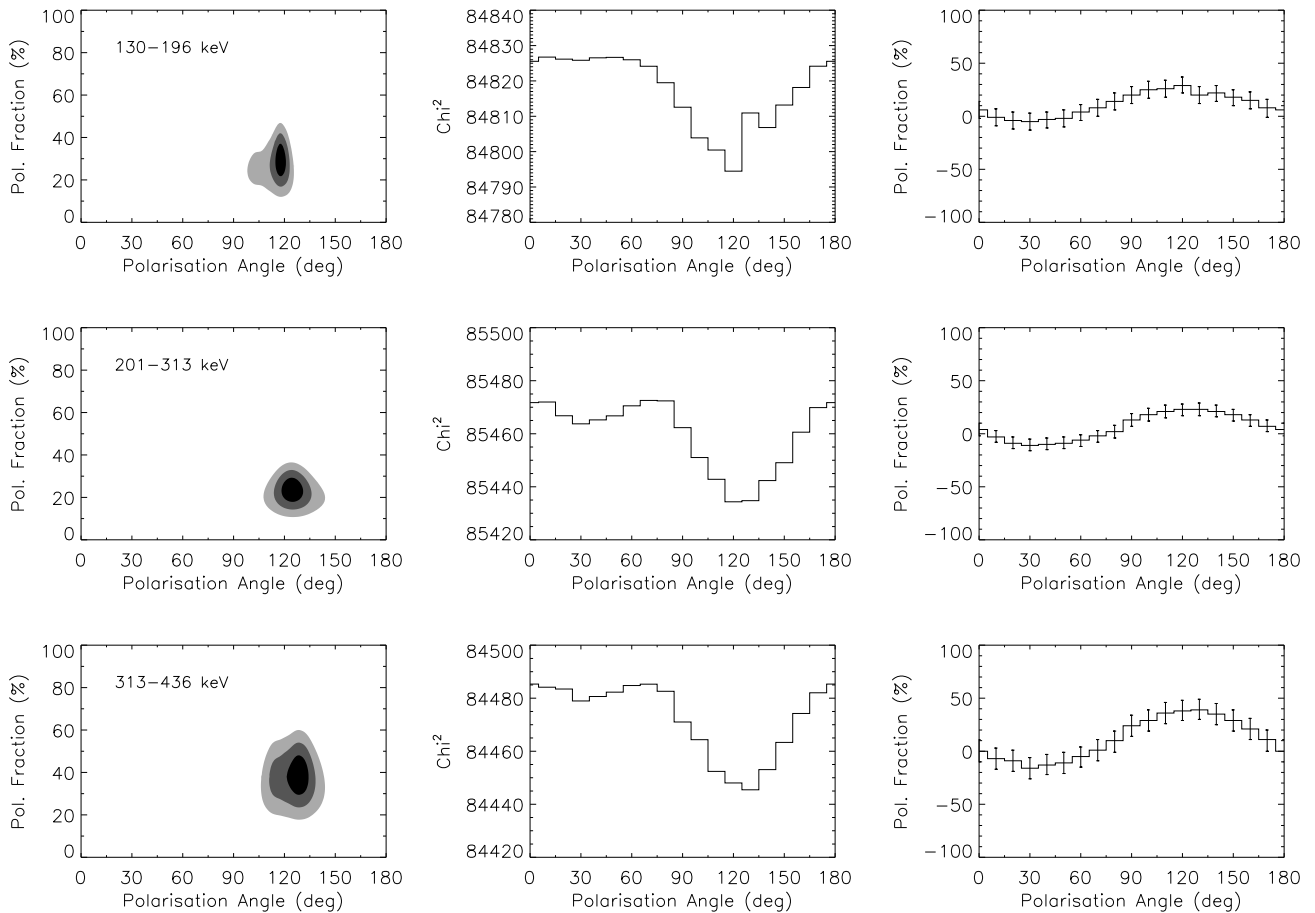


Figure 5. The same as Figure 2, for three narrower energy bands.

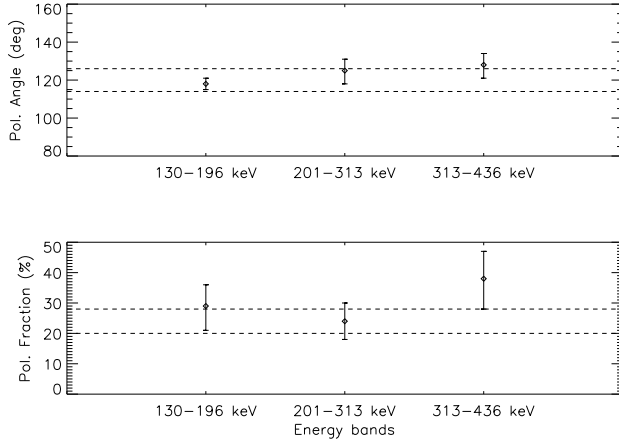


Figure 6. Evolution of the polarization parameters with energy for the total data set. Dashed lines represent the $1\text{-}\sigma$ uncertainty interval for the total data set best-fit values.

the incident flux is traced by the angle distribution of the diffused photons. This distribution can be reconstructed on the SPI detector plane, thanks to its 19 individual crystals. Considering the complexity of the polarimetry studies, it is crucial to ensure the reliability of the results, through the reliability of the reconstructed fluxes. This check has been done thanks to the spectral analysis of the same photons as those used in the Polarization analysis. This step testifies that the observed polarized emission comes from the Crab nebula.

Then, we have determined the characteristics of the polarized emission of the Crab nebula, with a robust signal-to-noise ratio, at $\text{PA} = 120^\circ \pm 6^\circ$ and $\text{PF} = 24 \pm 4\%$ and established their stability over the 16 years of *INTEGRAL* operations. Moreover, it has been shown that these values do not vary with energy, from 130 to 436 keV. Also, they are in good agreement with those obtained with the 2003 observations by Chauvin et al. (2013), *INTEGRAL* IBIS (Forot et al. 2008), PoGOLite+ (Chauvin et al. 2017), CZTI instrument on AstroSat (Vadawale et al. 2018) and SGD on Hitomi (Hitomi collaboration 2019), when they consider (as done here) the total (Pulsar + nebula) Crab emission. Lastly, our value is comparable to those reported in optical by Słowikowska et al. (2009). The polarization properties, even for a source known for its long term stability like the Crab, are most probably variable in space and time: indeed, a more complex behavior appears clearly as soon as instruments are able to realized spatially or phase resolved analyses (see for instance, Słowikowska et al. (2009)). However, the global measurements contain the dominant properties of the source and help to capture a macroscopic picture of this complex region.

The detection of a high polarization fraction is the definite argument for a synchrotron origin of the hard X-ray emission. Put together with radio and optical studies, this also proves that the same component produces photons from radio to $\sim \text{MeV}$ region. The unchanged polarization fraction, deduced from our analysis, reflects the well-known stability of the source. Concerning the second parameter, the measured polarization angle corresponds to an electric vector aligned with the spin axis of the central object (124° , Ng & Romani (2004)) and is also in line with the optical measurements (Słowikowska et al. 2009). The source steadiness is still more important in this case, since any variability of the angle weakens or even removes the observable information. Indeed, a variation

of the polarization angle smears the angular distribution of the scattered events, thus reducing the observed polarization fraction.

Harding & Kalapotharakos (2017) have developed a detailed simulation code to reproduce the expected emission from this kind of object, including polarization properties. They consider synchrotron radiation at optical to hard X-ray energies and provide phase-averaged and phase-resolved predicted fluxes, polarizations angles and polarization fractions. The predicted values cannot be directly compared to observations. However, the expected polarization fractions in the sub-Mev region range from 10 to 30 % depending on the assumed geometry, nicely similar to the values deduced from our observations. This demonstrates that simulation and data analysis works in the polarimetry domain are in the process of significantly improving our understanding of pulsar physics and high energy photon production in general.

Polarization measurements provide a complementary window particularly valuable to understand the mechanisms involved in the production of the high energy emission of compact objects. The Crab Pulsar and its nebula enjoy a special status in the hard X-ray domain. The stability of the spectral emission, in shape as well as in intensity, is advantageous, particularly for getting high signal-to-noise ratios by accumulating data over long periods, or offering in flight calibration facilities for high energy instruments. Our results show that it could serve as a reference source in the polarimetry domain also, from an instrumental as well as a modeling point of view.

ACKNOWLEDGMENTS

The *INTEGRAL* SPI project has been completed under the responsibility and leadership of CNES. We are grateful to ASI, CEA, CNES, DLR, ESA, INTA, NASA and OSTC for support.

APPENDIX

A. TESTS OF POLARIZATION TOOLS

The SPI polarimetric capacities rely on the Compton interactions of high energy photons in the detection plane. In the case of a linearly polarized flux, the azimuthal angle distribution of the Compton scattered photons is no longer isotropic. This means that the angular distribution of the diffused photons lays out a specific patterns on the detector plane, directly related to the polarization properties. Consequently, the polarization analysis relies on the SPI response, in the specific case of Compton events (or ME for Multiple events). It is thus important to check that this response is precisely known. This guarantees a reliable extraction of the Compton events, and also, permits to identify the spatial distributions corresponding to different polarized fluxes.

The SPI simulations used in the polarization analysis are based on TIMM (for The Integral Mass Model Ferguson et al. (2003)), translated from GEANT3 into the GEANT4 tool, with further improvements, including the anti-coincidence system configuration and the central mask pixel transparency (Chauvin et al. 2013). Each simulation is based on millions of photons, with a parametrable energy distribution probability (matching the analyzed source spectral shape), and randomly distributed over a large surface to ensure the illumination of the whole instrument. For one photon fired, all the information are stored (involved detectors, energy deposits,...). To finalize a run, the data are processed in the same way as the observational data.

We used instrumental data obtained during the ground calibration campaign, for a mono-energetic (unpolarized) radioactive source at 661 keV, to assess that the Geant4 simulations correctly reproduce

Table 1. Observations Log

Period Number	Tstart	Tstop	Useful duration	included revolutions
P1	2003-02-19	2003-02-27	446 ks	43-44-45
P2	2005-10-11	2011-10-07	1.94 Ms	365-422-483-541-605-665-727-774
P2 cont.				839-902-903-967-968-970-1089-1096
P3	2012-04-10	2014-10-06	1.82 Ms	1159-1160-1214-1221-1268-1269
P3 cont.				1327-1328-1387-1461-1462
P4	2015-03-06	2018-09-17	2.2 Ms	1515-1516-1598-1599-1661-1662-1723-1724
P4 cont.				1784-1785-1856-1857-1927-1928 -1999-2000

Table 2. Crab nebula best-fit parameters with the Band model. 0.5% systematic errors included.

Period	α_1	E_{ch}	α_2	χ^2 (dof)
P1 446 ks	2.00	601	2.22	77.01 (39)
P2 1.94 Ms	2.01	620	2.25	82.4 (39)
P3 1.82 Ms	2.0	602	2.32	71.9 (39)
P4 2.2 Ms	1.99	505	2.28	85.9 (39)
Tot	2.0	572.3	2.27	351.2 (165)

the instrument response for both single and multiple detector events. Since the GEANT4 software package ([Geant4 Collaboration 2003](#)) includes the polarization physics (as validated by [Mizuno et al. \(2005\)](#)), we activated this functionality in our code to get simulated count patterns for a set of polarization angles. This allows us to check that the spatial distributions of ME are in agreement when considering the unpolarized simulation. Moreover, it demonstrates that a polarized incident flux results in an anisotropy of the Compton event distribution on the detection plane. For instance, the difference between the unpolarized data mentioned above and a 20° polarized simulation has been evaluated to $\sim 20\%$ (see figures 4 and 5 in [Chauvin et al. \(2013\)](#)).

REFERENCES

- Band, D., Matteson, J., Ford, L., et al. 1993, ApJ, 413, 281
- Chauvin, M., Roques, J. P., Clark, D., & Jourdain, E. 2013, ApJ, 769, 137
- Chauvin, M., Florén, H. -G., Friis, M., et al. 2017, Sci. Rep., 7, 7816
- Dean, A. J., Clark, D. J., Stephen, J. B., et al. 2008, Science, 321, 1183

- Forot, M., Laurent, P., Grenier, I., et al. 2008, A&A, 688, L29
- Ferguson, C., Barlow, E. J., Bird, A. J. et al. 2003, A&A, 411, L19
- Geant4 Collaboration, Agostinelli, S., Allison, J., et al. 2003, NIMPA, 506, 250
- Harding, A. K., & Kalapotharakos, C. 2017, ApJ, 840, 73
- Hitomi Collaboration, Aharonian, F., Akamatsu, H., et al. 2018, PASJ, 70, 113
- Jourdain, E., & Roques, J. P. 2009, ApJ, 704, 17
- Mizuno, T., Kamae, T., Ng, J. S. T., et al. 2005, NIMPA, 540, 158
- Ng, C.-Y., & Romani, R. W. 2004, ApJ, 601, 479
- Roques, J. P., Schanne, S., Von Kienlin, A., et al, 2003, A&A, 411, L91
- Roques, J. P., & Jourdain, E. 2019, ApJ, 870, 92
- Słowikowska A., Kanbach G., Kramer M., & Stefanescu A., 2009, MNRAS, 397, 103
- Sturner S. J., Shrader C. R., Weidenspointner G., et al, 2003, A&A, 411, L81
- Vadawale, S. V., Chattopadhyay, T., Mithun, N. P. S., et al., 2018, Nature astron., 2, 50
- Vedrenne, G., Roques, J.P., Schonfelder, V., et al, 2003, A&A, 411, L63